

Deflectometry for phase retrieval using a composite fringe

TONGCHUAN LIU¹, CANLIN ZHOU^{1*}, YEPENG LIU¹, SHUCHUN SI¹, ZHENKUN LEI²

¹School of Physics, Shandong University, Jinan 250100, China

²Department of Engineering Mechanics, Dalian University of Technology, Dalian 116024, China

*Corresponding author: canlinzhou@sdu.edu.cn

An improved deflectometry for wavefront measurement using a composite fringe is proposed to reduce the projection fringes and improve the accuracy. The single composite fringe contains four fringes in different directions. It goes through the tested objects and then is captured by a CCD camera. Two high frequency orthogonal fringe patterns and two single period orthogonal fringe patterns can be obtained from the composite fringe by fast Fourier transform. The unwrapping of the wrapped phase of the high frequency fringe is accomplished by the corresponding single period fringe using a heterodyne method. The wavefront is reconstructed by the integration of partial derivatives. Using only one fringe, the proposed method is more applicable to dynamic wavefront measurement. The experimental results demonstrate that the proposed method can retrieve the complex wavefronts more accurately.

Keywords: wavefront measurement, fringe analysis, phase retrieval, fast Fourier transform (FFT), multi-frequency heterodyne principle.

1. Introduction

Many methods for wavefront measurement have been presented so far. They measure the phase directly or measure the wavefront slope. Measuring the phase directly has a high accuracy, but it is not suitable for measuring objects with complex shapes. Measuring the wavefront slope can solve the problem, but it requires coherent illumination and a precise positioning of the optical setup.

A simple technique for measuring the wavefront slopes, consisting of a LCD monitor and a CCD camera, has been developed in the last decade [1, 2]. The conventional fringe algorithms are used to extract the deflections introduced by the tested object modifying the reference fringe pattern. However, for the general wavefront, two partial derivatives of the phase are needed to recover the desired wavefront. Two fringe patterns are displayed and captured successively in orthogonal directions. It is not suitable for dynamic measurements. FLORES *et al.* proposed to utilize a two-dimensional additive

fringe to extend the one-dimensional deflectometry to two-dimensional case [3]. It has an advantage of measuring smooth wavefront slopes by one-shot deflectometry. But phase unwrapping must be carried out before wavefront information can be deduced from the partial derivatives of the phase. Encountering an object with a complex shape, phase unwrapping will become a difficult procedure. CANABAL and ALONSO [1] employed the TPU (temporal phase unwrapping) method [4–6], where the unwrapping is carried out along the time axis. CASTILLO *et al.* [7] proposed the technique for wavefront measurement of flame flux by combining the color fringe pattern and the temporal phase unwrapping method [8]. These methods need the manipulation of various images, which do not meet the requirements of dynamic measurement.

Inspired by GARCÍA-ISÁIS and OCHOA [9], we get four fringe patterns from a composite fringe to solve this problem. Different from the method proposed by García-Isáis, we develop a single composite fringe containing four fringes in different directions. By calculating, we get two high frequency orthogonal fringe patterns and two single period orthogonal fringe patterns. Making use of a heterodyne principle [10–13], we get simultaneously two accurate wavefront slope components from the orthogonal fringe patterns. After integration, we can obtain the results with a high accuracy. Though our method resembles the one proposed in [9], it is extended to the two-direction from the original one-direction, which meets the requirements of phase unwrapping in the wavefront measurement.

The paper is organized as follows. Section 2 introduces the principle of the system. Section 3 shows the procedure of the experiment. Section 4 presents the experimental results. Section 5 discusses different results and summarizes this paper.

2. Fringe analysis

Suppose that we have a fringe pattern displayed in a LCD across the plane (x, y) with fringes along the y -direction. The optical path lengths will change if we place a pure phase object in front of the fringe pattern. The rays will be deflected by an angle $\alpha = \partial W(x, y)/\partial x$, if the phase is inhomogeneous in the x -direction; $W(x, y)$ is the optical path length accumulated by a ray traveling through the phase object at the position (x, y) .

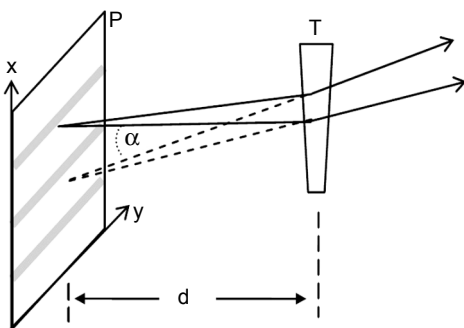


Fig. 1. One-dimensional deflectometry.

The fringes will appear shifted in the x -direction by a distance $\alpha d \approx (\partial W(x, y)/\partial x)d$ while the distance of the test object to the displayed pattern is d (as shown in Fig. 1).

Without loss of generality, we can suppose the undistorted fringe pattern is as follows:

$$I(x, y) = I_0 \left[1 + \cos(2\pi fx) \right] \quad (1)$$

where f is the carrier frequency. The intensity distribution seen through the phase object will be as follows:

$$I(x, y) = I_0 \left[1 + \cos \left(2\pi fx + 2\pi fd \frac{\partial W(x, y)}{\partial x} \right) \right] \quad (2)$$

However, to reconstruct the wavefront $W(x, y)$, we need to obtain the partial derivatives $\partial W(x, y)/\partial x$ and $\partial W(x, y)/\partial y$.

Using a computer, we generate a composite pattern to be displayed in a LCD given by

$$I(x, y) = \frac{G}{8} \left\{ 4 + \cos(2\pi fx) + \cos(2\pi fy) + \right. \\ \left. + \cos \left[2\pi(1-f)x + 2\pi fy \right] + \cos \left[2\pi fx + 2\pi(1+f)y \right] \right\} \quad (3)$$

where f is the carrier frequency, G is the constant that represents the amplitude value, (x, y) are the normalized pixel coordinates, and $I(x, y)$ is the image with its gray levels in the range $[0, G]$. We can see that the pattern given by Eq. (3) comprises the sum of four fringe patterns: one with vertical fringes, another with horizontal fringes, and the last two with fringes almost at 45° and 135° . If the carrier terms are written as follows:

$$c_x(x, y) = 2\pi fx, \quad c_y(x, y) = 2\pi fy \quad (4)$$

$$c_{xy1}(x, y) = 2\pi(1-f)x + 2\pi fy \quad (5)$$

$$c_{xy2}(x, y) = 2\pi fx + 2\pi(1+f)y \quad (6)$$

then the following relations hold,

$$c_{xy1}(x, y) + c_x(x, y) - c_y(x, y) = 2\pi x \quad (7)$$

$$c_{xy2}(x, y) - c_x(x, y) - c_y(x, y) = 2\pi y \quad (8)$$

The cosines in formulas (7) and (8) are one period vertical and horizontal fringes.

The intensity profile that we will obtain after the fringe in Eq. (3) goes through the object will be given by

$$i = a + b \left[\cos(c_x + \varphi^x) + \cos(c_y + \varphi^y) + \cos(c_{xy1} + \varphi^{xy1}) + \cos(c_{xy2} + \varphi^{xy2}) \right] \quad (9)$$

where a and b are the background and amplitude terms that depend on the LCD, respectively, φ^x , φ^y , φ^{xy1} and φ^{xy2} are the phase functions related to the wavefront.

As presented in [9], the Fourier transform of Eq. (9) can be expressed as

$$\begin{aligned} I(u, v) = & A(0, 0) + D_x(u - f, v) + D_y(u, v - f) + \\ & + D_{xy1}(u + f - 1, v - f) + D_{xy2}(u - f, v - f - 1) + \\ & + D_x^*(u + f, v) + D_y^*(u, v + f) + \\ & + D_{xy1}^*(u - f + 1, v + f) + D_{xy2}^*(u + f, v + f + 1) \end{aligned} \quad (10)$$

where (u, v) are the frequency coordinates. It consists of nine spectra centered on frequencies $(0, 0)$, $(f, 0)$, $(0, f)$, $(1 - f, f)$, $(f, f + 1)$, $(-f, 0)$, $(0, -f)$, $(f - 1, -f)$ and $(-f, -f - 1)$. We only choose D_x , D_y , D_{xy1} and D_{xy2} to filter. We can separate these terms accurately by a band-pass filter, and then transform them into the space domain by the inverse Fourier transform. By computing the phase angle of these quantities, we can obtain the phase maps of four fringe patterns as follows:

$$\phi^x = \left[C_x + \varphi'^x \right]_{\text{mod } 2\pi} = \arctan \left\{ \frac{\text{Im} \left[D_x(u - f, v) \right]}{\text{Re} \left[D_x(u - f, v) \right]} \right\} \quad (11a)$$

$$\phi^y = \left[C_y + \varphi'^y \right]_{\text{mod } 2\pi} = \arctan \left\{ \frac{\text{Im} \left[D_y(u, v - f) \right]}{\text{Re} \left[D_y(u, v - f) \right]} \right\} \quad (11b)$$

$$\phi^{xy1} = \left[C_{xy1} + \varphi'^{xy1} \right]_{\text{mod } 2\pi} = \arctan \left\{ \frac{\text{Im} \left[D_{xy1}(u + f - 1, v - f) \right]}{\text{Re} \left[D_{xy1}(u + f - 1, v - f) \right]} \right\} \quad (11c)$$

$$\phi^{xy2} = \left[C_{xy2} + \varphi'^{xy2} \right]_{\text{mod } 2\pi} = \arctan \left\{ \frac{\text{Im} \left[D_{xy2}(u - f, v - f - 1) \right]}{\text{Re} \left[D_{xy2}(u - f, v - f - 1) \right]} \right\} \quad (11d)$$

The wrapped differences of ϕ^{xy1} , ϕ^{xy2} , ϕ^x and ϕ^y are shown as:

$$\phi_1^w = \arctan \left[\frac{\sin(\phi^{xy1} + \phi^x - \phi^y)}{\cos(\phi^{xy1} + \phi^x - \phi^y)} \right] \quad (12)$$

$$\phi_2^w = \arctan \left[\frac{\sin(\phi^{xy2} - \phi^x - \phi^y)}{\cos(\phi^{xy2} - \phi^x - \phi^y)} \right] \quad (13)$$

As presented in Eqs. (7) and (8), each of the wrapped differences consists of only one period and is within the range 0 to 2π . To get ϕ_1 and ϕ_2 , the unwrapped function of the low frequency wrapped function ϕ_1^w and ϕ_2^w , the following relations are satisfied:

$$\phi_1 = (c_{xy1} + c_x - c_y) + (\phi^{xy1} + \phi^x - \phi^y) \quad (14)$$

$$\phi_2 = (c_{xy2} - c_x - c_y) + (\phi^{xy2} - \phi^x - \phi^y) \quad (15)$$

Using Eq. (7) and Eq. (8) in Eq. (14) and Eq. (15), we obtain

$$\phi_1(x, y) = 2\pi x + \phi^{E1}(x, y) \quad (16)$$

$$\phi_2(x, y) = 2\pi y + \phi^{E2}(x, y) \quad (17)$$

where $\phi^{E1} = \phi^{xy1} + \phi^x - \phi^y$ and $\phi^{E2} = \phi^{xy2} + \phi^x - \phi^y$ represent the equivalent phases of the phase differences. Then, what we have obtained are two single period fringe patterns [9].

The multifrequency heterodyne principle can provide an accurate phase map because it can calculate the phase value of every pixel independently [13]. The unwrapped phase $\phi(x)$ is calculated by adding the phase function $\phi_1(x)$ and the order function $O_1(x)$ multiplied by 2π

$$\phi(x) = \phi_1(x) + O_1(x) \times 2\pi \quad (18)$$

Since we have the phase maps of two single period fringe patterns and two related high frequency fringe patterns, we can get two accurate orthogonal phase maps by Eq. (18). They are the partial derivatives $\partial W(x, y)/\partial x$ and $\partial W(x, y)/\partial y$.

Two accurate components of the ray deflection are obtained, then we can reconstruct the wavefront because it will be the solution of a Poisson equation with the source term $\partial^2 W/\partial x^2 + \partial^2 W/\partial y^2$ resulting from the derivation of the vector $(\partial W(x, y)/\partial x, \partial W(x, y)/\partial y)$.

The integration of the partial derivatives $\partial W(x, y)/\partial x$ and $\partial W(x, y)/\partial y$ is equivalent to finding the function $f(x, y)$ that is the solution of the Poisson equation $\nabla^2 f(x, y) = g(x, y)$ [3], while $f(x, y)$ can be written as

$$f(x, y) = -\left(\frac{L}{\pi}\right)^2 \sum_{k=1}^L \sum_{n=1}^L \frac{d_{kn}}{n^2 + k^2} \sin\left(\frac{\pi kx}{L}\right) \sin\left(\frac{\pi ny}{L}\right) \quad (19)$$

where

$$d_{kn} = \frac{1}{L^2} \int_0^{2L} \int_0^{2L} g(x, y) \sin\left(\frac{\pi kx}{L}\right) \sin\left(\frac{\pi ny}{L}\right) dx dy \quad (20)$$

3. Experiments

Now, we will describe some experiments and practical suggestions for the above procedure.

The two-dimensional composite fringe pattern described by Eq. (3) was displayed in a LCD. We set $f = 20$ and $G = 255$. Our tested object was a convex lens with a diameter of 7 cm as shown in Fig. 2. The lens was 5 cm distant from the LCD. The camera used for acquiring the images was at a distance of the order of 100 cm from the LCD.

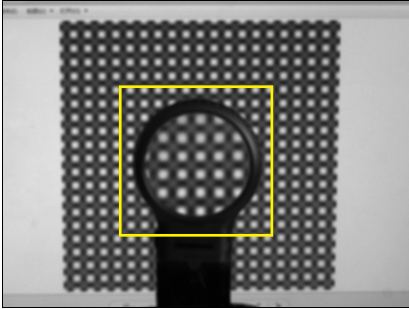


Fig. 2. The tested convex lens.

Figure 3 shows the frequency spectrum of the acquired pattern. The nine bright spots are clearly visible, therefore it is easy to locate their position. Multiplying the FFT result with a Hanning filter of radius 10, centered on the frequency coordinates $(30, 0)$, $(0, 23)$, $(-30, 23)$ and $(30, 23)$ shown in the circles, and calculating the four inverse FFTs, we have obtained four wrapped phases given by Eq. (7) and shown in Fig. 4.

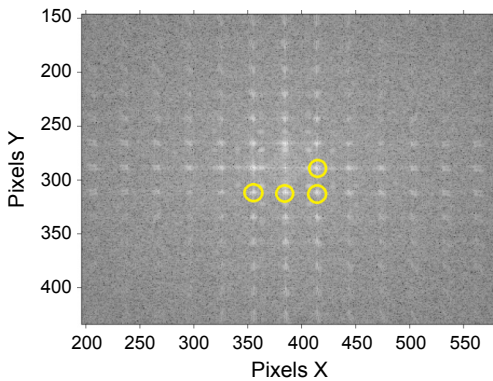


Fig. 3. Frequency spectrum of the acquired pattern.

Using Eqs. (16) and (17), we obtain the phase maps of two fringe patterns without unwrapping as follows:

$$c_x(x, y) = 2\pi x, \quad c_y(x, y) = 2\pi y \quad (21)$$

Taking advantage of the multifrequency heterodyne principle, we can obtain the accurate phase maps of two orthogonal fringe patterns with the phase maps of two single period fringe patterns and two related high frequency fringe patterns.

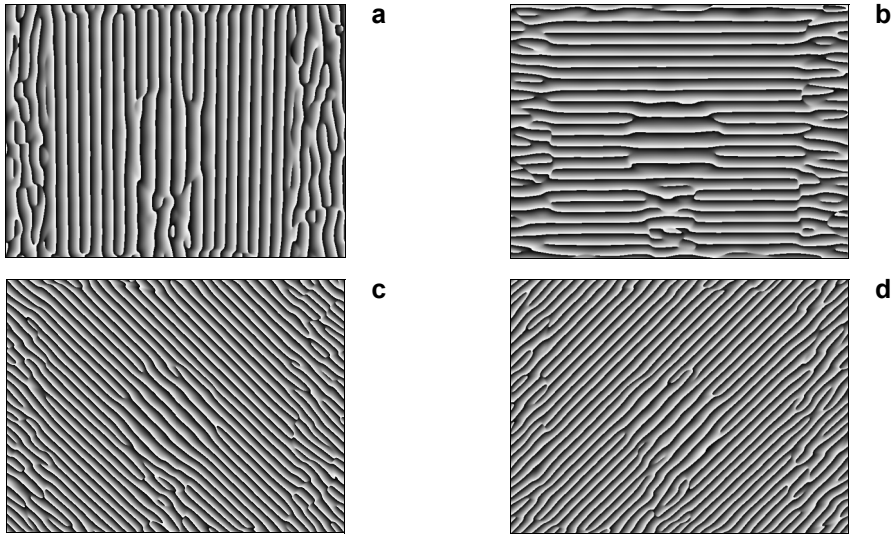


Fig. 4. Wrapped phase components obtained from the Fourier spectrum. Horizontal (a), vertical (b), slope upper right (c), and slope bottom right (d).

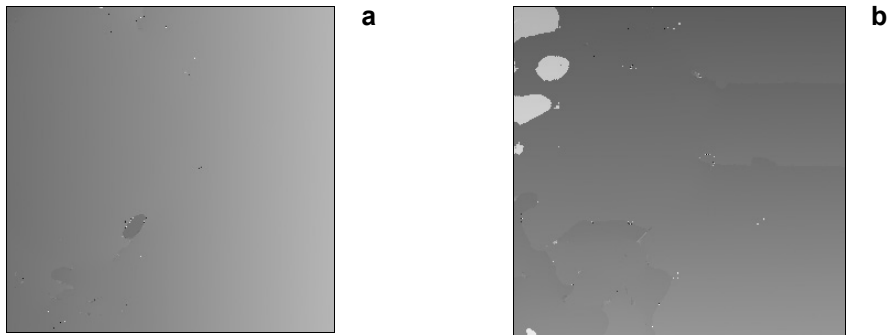


Fig. 5. The unwrapped maps of $\partial W(x, y)/\partial x$ (a), and $\partial W(x, y)/\partial y$ (b).

In order to avoid boundary effects, we choose a region in the middle as shown in Fig. 2. The unwrapped maps of $\partial W(x, y)/\partial x$ and $\partial W(x, y)/\partial y$ are shown in Fig. 5.

As presented in Section 2, with the value of the vector $(\partial W(x, y)/\partial x, \partial W(x, y)/\partial y)$, obtained above, we can calculate $\nabla^2 W(x, y)$. Basing on the result of the numerical integration of the Poisson equation with $\nabla^2 W(x, y)$, we reconstructed the wavefront $W(x, y)$.

4. Results

We reconstruct the wavefronts by Flores algorithm, García-Isáis algorithm and the proposed algorithm separately. As shown in Figs. 6a–6c, the central areas corresponding to the convex lens are smooth and similar. By comparison of the results, we can see that all the methods can retrieve the wavefronts of the convex lens well.

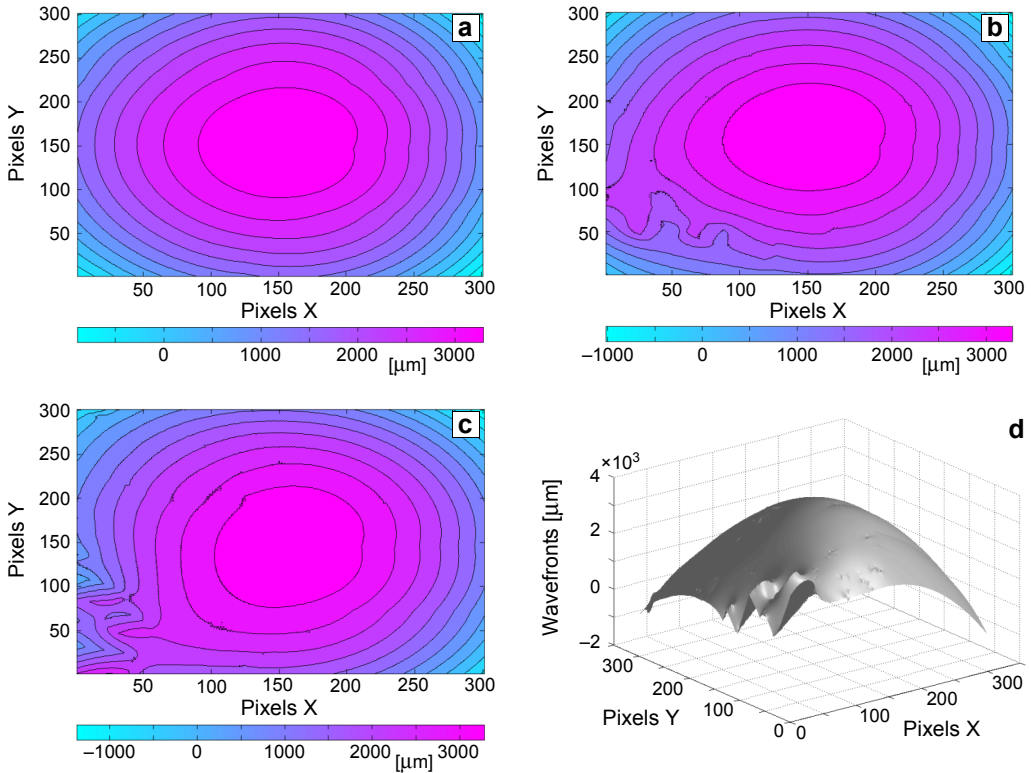


Fig. 6. Wavefronts obtained by Flores algorithm (a), by García-Isáis algorithm (b), and by the proposed algorithm (c). 3D display of the wavefronts recovered by the proposed algorithm (d).

The contrasts are not obvious when the tested object has a simple shape. The computational times are 0.7216, 0.7286 and 0.7360 s. There is little difference among them.

The 3D display of the wavefronts recovered by the proposed algorithm is shown in Fig. 6d. It conforms to the shape of the tested lens. This confirms the practicability of the proposed algorithm.

Lacking the theoretical value, we simulate the above experiment by MATLAB. We choose an area in the center of the convex lens to measure. After being normalized, the mean square errors obtained by Flores algorithm, García-Isáis algorithm and the proposed algorithm are 0.3153, 0.3063 and 0.3005. The computational times are 0.2843, 0.2872, and 0.2896 s. At the longest computational time, the proposed algorithm has the highest accuracy. The comparisons of them are not obvious. To contrast the three algorithms distinctly, we do another experiment on a complex bottle as shown in Fig. 7.

Since the pattern in the middle of the bottle is a semicircle and the matter is isotropic, the wavefronts should have the same structure in the middle. The differences in the structures of the wavefronts obtained by Flores algorithm, García-Isáis algorithm and the proposed algorithm are shown in Figs. 8a–8c, respectively. The contrasts among

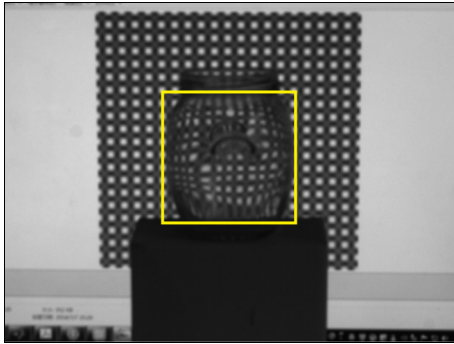


Fig. 7. The tested complex bottle.

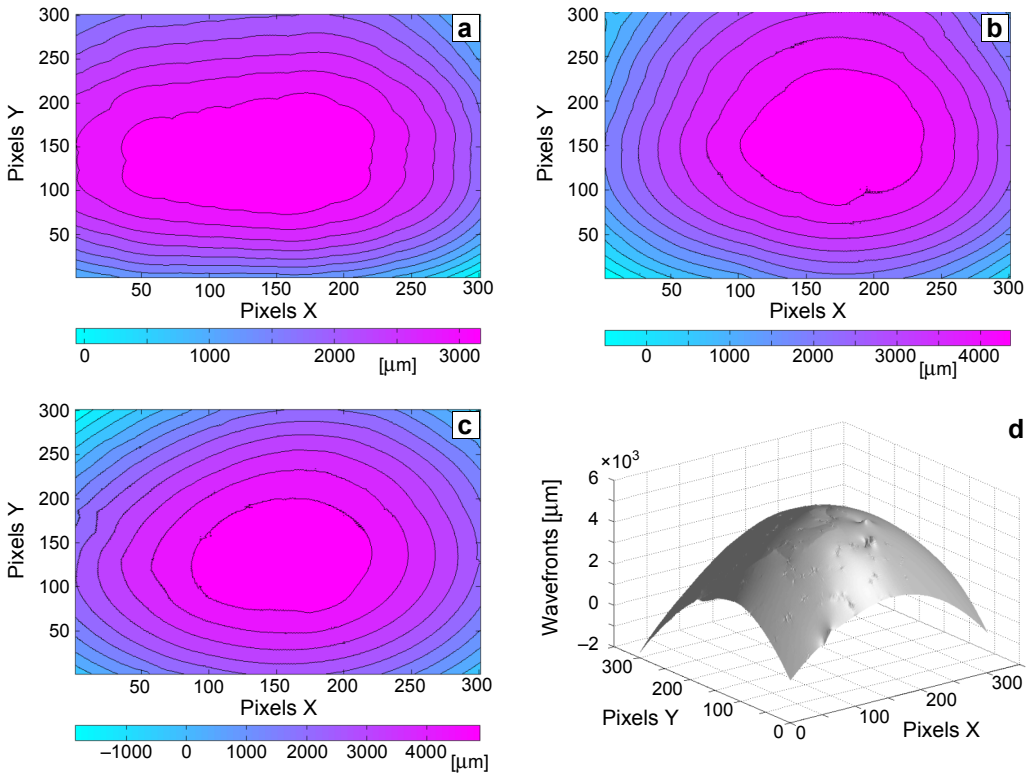


Fig. 8. Phase change obtained by Flores algorithm (a), by García-Isáis algorithm (b), by the proposed algorithm (c). 3D display of the wavefronts recovered by the proposed algorithm (d).

the figures are obvious. The contour lines in Fig. 8a are nearly rectangles which are very different from the bottle. The contour lines in Fig. 8b are rounder. García-Isáis algorithm is more accurate. The contour lines in Fig. 8c are the roundest. The proposed algorithm is the most accurate. The 3D display of the wavefronts recovered by the proposed algorithm is shown in Fig. 8d. It also conforms to the structure of the bottle. The computational times are 0.7241, 0.7312 and 0.7364 s. The complexity of the tested

object influences the computational times little, however, it influences the accuracy obviously. The experiment demonstrates that the proposed method can retrieve the complex wavefronts more accurately.

The proposed algorithm unwraps the wrapped phases $\partial W(x, y)/\partial x$ and $\partial W(x, y)/\partial y$ by the multifrequency heterodyne method. García-Isáis algorithm unwraps the wrapped phases $\partial W(x, y)/\partial x$ in the same way, however, it unwraps the wrapped phases $\partial W(x, y)/\partial y$ by the general spatial method. Since $\partial W(x, y)/\partial y$ has errors, the reconstructed wavefronts $\nabla^2 W(x, y)$ have a low accuracy. The accuracy of Flores algorithm is much lower. It is because the algorithm only separates two orthogonal fringes from the composite fringe by FFT, and the unwrapping procedure of a wrapped phase is very simple. When the object has a complex shape, the accuracy reduces most.

The more complex the algorithm is, the more computational time it uses. The differences in computational times are small. Taking advantage of multi-threading and parallel processing, GPU (graphic processing unit) algorithm can speed up the processes of the multifrequency heterodyne method [14]. Then the proposed algorithm will use less computational time and apply to the dynamic wavefront measurement better.

Using only one fringe, the proposed method makes it possible to measure dynamic wavefronts. In general, it can retrieve the wavefronts quickly and accurately. Especially, when the tested object has a complex shape, the proposed method can improve the accuracy greatly.

5. Conclusions

By a composite fringe containing four fringe patterns, we get the accurate phase maps of two accurate orthogonal fringe patterns. Basing on the phase maps, we obtain the accurate wavefront patterns. The proposed algorithm is more applicable to dynamic wavefront measurement. It can retrieve the complex wavefronts more accurately.

Acknowledgments – This work was supported by the National Nature Science Foundation of China (No. 11172054), the support is gratefully acknowledged.

References

- [1] CANABAL HA., ALONSO J., *Automatic wavefront measurement technique using a computer display and a charge coupled device camera*, *Optical Engineering* **41**(4), 2002, pp. 822–826.
- [2] LEGARDA-SAENZ R., ESPINOSA-ROMERO A., *Wavefront reconstruction using multiple directional derivatives and Fourier transform*, *Optical Engineering* **50**(4), 2011, article 040501.
- [3] FLORES J.L., BRAVO-MEDINA B., FERRARI J.A., *One-frame two-dimensional deflectometry for phase retrieval by addition of orthogonal fringe patterns*, *Applied Optics* **52**(26), 2013, pp. 6537–6542.
- [4] YANJUN FU, YONGLONG WANG, JIANFENG WU, GUANGYU JIANG, *Dual-frequency fringe Fourier transform profilometry based on defocusing*, *Optics Communications* **295**, 2013, pp. 92–98.
- [5] YAJUN WANG, LAUGHNER J.I., EFIMOV I.R., SONG ZHANG, *3D absolute shape measurement of live rabbit hearts with a superfast two-frequency phase-shifting technique*, *Optics Express* **21**(5), 2013, pp. 5822–5832.

- [6] KAI LIU, YONGCHANG WANG, LAU D.L., QI HAO, HASSEBROOK L.G., *Dual-frequency pattern scheme for high-speed 3-D shape measurement*, Optics Express **18**(5), 2010, pp. 5229–5244.
- [7] CASTILLO O.E., LEGARDA-SÁENZ R., FLORES J.L., GARCIA-TORALES G., *Measurement of phase objects by the use of color phase-shifting technique*, Proceedings of SPIE **8867**, 2013, pp. 886710–886716.
- [8] HUNTLEY J.M., SALDNER H., *Temporal phase-unwrapping algorithm for automated interferogram analysis*, Applied Optics **32**(17), 1993, pp. 3047–3052.
- [9] GARCÍA-ISÁIS C.A., OCHOA N.A., *One shot profilometry using a composite fringe pattern*, Optics and Lasers in Engineering **53**, 2014, pp. 25–30.
- [10] YANMING CHEN, YUMING HE, ERYI HU, HONGMAO ZHU, *Deformation measurement using dual-frequency projection grating phase-shift profilometry*, Acta Mechanica Solida Sinica **21**(2), 2008, pp. 110–115.
- [11] CHAO ZUO, QIAN CHEN, GUOHUA GU, SHIJIE FENG, FANGXIAOYU FENG, RUBIN LI, GUOCHEN SHEN, *High-speed three-dimensional shape measurement for dynamic scenes using bi-frequency tripolar pulse-width-modulation fringe projection*, Optics and Lasers in Engineering **51**(8), 2013, pp. 953–960.
- [12] ZHENZHONG XIAO, OICHOO CHEE, ANAND ASUNDI, *An accurate 3D inspection system using heterodyne multiple frequency phase-shifting algorithm*, Physics Procedia **19**, 2011, pp. 115–121.
- [13] REICH C., RITTER R., THESING J., *White light heterodyne principle for 3D-measurement*, Proceedings of SPIE **3100**, 1997, pp. 236–244.
- [14] KARPINSKY N., HOKE M., CHEN V., ZHANG S., *High-resolution, real-time three-dimensional shape measurement on graphics processing unit*, Optical Engineering **53**(2), 2014, article 024105.

*Received March 9, 2014
in revised form July 12, 2014*